Inertial Taylor columns on a beta plane

By MICHAEL S. McCARTNEY

Woods Hole Oceanographic Institution

The effect of variable Coriolis parameter on the formation of inertial Taylor columns is determined for the case of a two-layer fluid with moderate stratification. Analytic solutions of the inertial, quasi-geostrophic, β-plane equations are obtained. As a special case, solutions corresponding to a single-layer, homogeneous fluid are also obtained. When both layer velocities are retrograde (westward), the effect of β is to limit the horizontal extent of the disturbance due to the bump. When both layer velocities are prograde (eastward), an extensive meandering wake is found downstream of the bump. Associated with this wake can be large stationary cyclonic and anti-cyclonic eddies. The meander amplitudes in the two layers are typically nearly the same. In both the retrograde and prograde cases, the strength of the disturbance to the flow above the bump is less in the upper layer compared with the lower, indicating an attenuation in the vertical due to stratification. For a counter-flow situation, the solutions are complicated by the possibility of a stationary baroclinic wave, one that would exist even for $\beta = 0$. In all the situations in which a meandering wake is formed, there is a wave-drag force on the bump. Some laboratory experiments corresponding to the single-layer solutions are described.

1. Introduction

Taylor columns have received much attention, both theoretical and experimental, since Hide (1961) speculated that Jupiter's Great Red Spot might be an example of one with a planetary length scale. Nearly all the theoretical works to date have been restricted to uniformly rotating systems (f plane), and thus to geophysical problems of rather small horizontal length scales: small enough that the latitudinal variation of Coriolis parameter does not affect the dynamics. For quite a few problems of interest (e.g. ocean currents flowing over seamounts, atmospheric winds flowing over mountains, or Jupiter's Great Red Spot), horizontal length scales are too large for this restriction to be made. In the present work, the lowest-order effect of variable Coriolis parameter on Taylor-column formation will be examined by looking at the flow over a bump on a β plane.

In the f-plane formulation, the full gamut of quasi-geostrophic problems has been considered. In table 1, these problems and the present investigation are summarized. As the table indicates, the only previous worker who examined the effect of β was Ingersoll (1969), who considered the limit $b \to \infty$ for a retrograde (westward) basic current in a homogeneous fluid. Hogg (1973) is the only author

Author	System	Type of quasi-geostrophy	Parameter ranges		
Grace (1927) Stewartson (1953, 1967)	Homogeneous fluid f plane	Time-dependent (initial-value problem)	$\epsilon = 0$ $h_0 = O(1)$ $S = 0$	$E^{\frac{1}{2}} = 0$ $b = 0$	
Jacobs (1964)	Homogeneous fluid f plane	Viscous (horizontal and vertical)	$\epsilon = 0$ $h_0 = O(1)$ $S = 0$	$E^{\frac{1}{2}} = 0$ $b = 0$	
Ingersoll (1969)	Homogeneous fluid (i) f plane (ii) β plane	Inertial	$\epsilon \ll 1$ $h_0 = O(\epsilon)$ $S = 0$	$E^{\frac{1}{2}} = 0$ (i) $b = 0$ (ii) $b \to \infty$ (retrograde)	
Vaziri & Boyer (1971)	Homogeneous fluid f plane	Inertial with bottom friction	$\epsilon \sim E_v^{\frac{1}{2}} \ll 1$ $h_0 = O(\epsilon)$ $S = 0$	$E_h^{\frac{1}{2}} = 0$ $b = 0$	
McCartney (1972)	Homogeneous fluid β plane	Inertial	$\epsilon \ll 1$ $h_0 = O(\epsilon)$ $S = 0$	$E^{\frac{1}{2}} = 0$ $b \leqslant O(1)$	
Hogg (1973)	Linearly stratified fluid f plane	Inertial	$\epsilon \ll 1$ $h_0 = O(\epsilon)$ $S \leqslant O(1)$	$E^{\frac{1}{2}} = 0$ $b = 0$	
Huppert (1974)	(i) Homogeneous fluid (ii) Linearly stratified fluid f plane	Inertial	$\epsilon \ll 1$ $h_0 = O(\epsilon)$ (i) $S = 0$ (ii) $S \leqslant O(1)$	$E^{\frac{1}{2}} = 0$ $b = 0$	
McCartney (present work, including the material of McCartney (1972) as a special case)	Two-layer stratified fluid β plane	Inertial	$\epsilon \ll 1$ $h_0 = O(\epsilon)$ $S \geqslant O(1)$	$E^{\frac{1}{2}} = 0$ $b \leqslant O(1)$	

TABLE 1. Summary of theoretical Taylor-column studies

thus far to publish results for a stratified fluid (see Huppert (1974) for a discussion of Hogg's work); and his results are for an f plane.

The specific model considered in the present work is that of a two-layer fluid on a β plane. The basic geometry is shown in figure 1. The Coriolis parameter

$$f(Y) = f(0) + \beta Y \equiv f_0 + \beta Y.$$

Y is the poleward co-ordinate. The following non-dimensional parameters are of significance:

$$\epsilon \equiv U_0/(f_0 L), \quad E_v \equiv \nu_v/(f_0 H^2), \quad E_h \equiv \nu_h/(f_0 H^2),$$
$$b \equiv \beta L^2/U_0 = \beta L/(f_0 \epsilon), \quad h_0 \equiv h_0'/H,$$
$$\delta \equiv H/L, \quad S \equiv gH\Delta\rho/(f_0^2 \rho_0 L^2) = \delta^2 N^2/f_0^2,$$
$$d = d'/H.$$

ϵ is a Rossby number. E_v and E_h are respectively the vertical and horizontal Ekman numbers. b is a measure of the dynamic importance of β, small b ($\ll 1$)
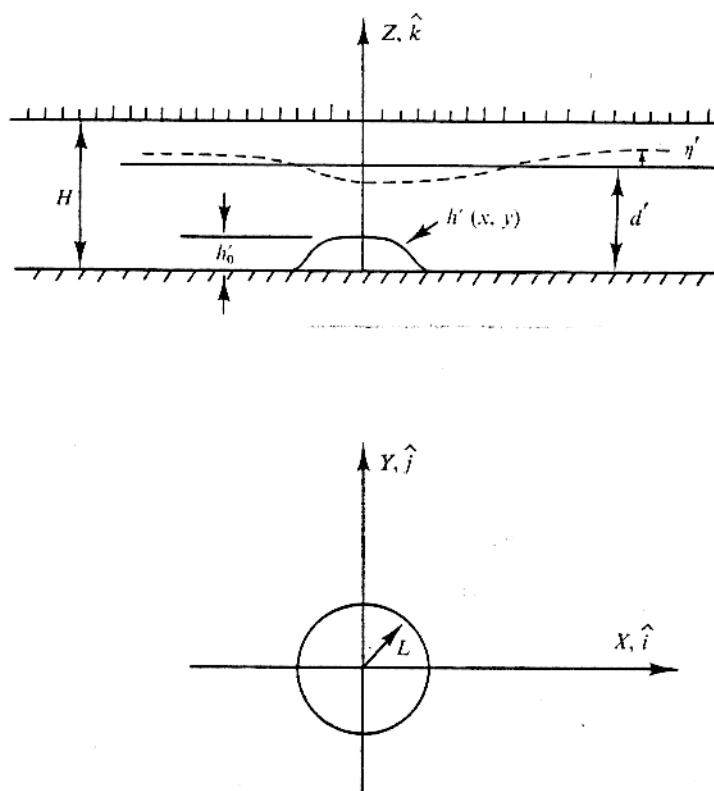
FIGURE 1. System geometry. (a) East–west section along $Y = 0$. ——, undisturbed interface; –––, disturbed interface. (b) Top view. Y is the poleward co-ordinate.

implying, in some sense, that β effects are unimportant. h_0 is the maximum fractional height of the isolated topographic feature $h'(X, Y)$. δ is the ratio of the total fluid depth H to the horizontal scale L of the bump. S is a measure of the dynamic importance of the stratification, small S ($\ll 1$) implying, in some sense, that stratification can be neglected. d is a measure of the lower-layer depth fraction. In these definitions the following quantities are used: ν_v and ν_h are, respectively, the vertical and horizontal kinematic eddy-viscosity coefficients; $U_0 = [d\mathcal{U}_1^2 + (1-d)\mathcal{U}_2^2]^{\frac{1}{2}}$ is an r.m.s. scaling velocity, based on the upper- and lower-layer typical velocities $\mathcal{U}_2$ and $\mathcal{U}_1$, respectively; $N^2 = g\Delta\rho/(\rho_0 H)$ is the Brunt–Väisälä frequency squared, based on the average density $\rho_0 = d\rho_1 + (1-d)\rho_2$, gravity g and the density difference $\Delta\rho = \rho_1 - \rho_2$; d' is the interface height above the bottom at $Y = 0$, when there is no bump. The interface height Z_{1n} is written as $Z_{1n} = d' + \eta'(x, y)$, with $\eta'(x, 0) = 0$, when there is no bump. The velocities far from the bump in each layer are uniform and zonal with magnitudes $\mathcal{U}_2$ and $\mathcal{U}_1$.

The parameter ranges considered in the previous works, and in the present, are included in the summary in table 1. Those authors who have the entries $E^{\frac{1}{2}} = 0$ retained neither vertical nor horizontal friction, while Jacobs (1964) had $E_v = E_h = E$.

In §2 the governing equations for the two layers are reduced to a single

manageable equation. In § 3 the general character of the solutions to this equation is discussed. The simplest solutions, those for $\mathscr{U}_1 < 0$ and $\mathscr{U}_2 < 0$ (i.e. westward currents: retrograde), are described in § 4. In § 5 the more complex solutions, those for $\mathscr{U}_1 > 0$ and $\mathscr{U}_2 > 0$ (i.e. eastward currents: prograde), are described. In both § 4 and § 5, solutions corresponding to a single-layer homogeneous fluid are obtained by taking the limit $S \to \infty$, in which the interface acts as a horizontal rigid lid. Some laboratory experimental results, related to the homogeneous fluid case, are described in § 6. The relationship between these theoretical and experimental results and some oceanic situations is discussed in § 7.

2. Governing equations for the two layers

We adopt the following non-dimensionalization scheme: horizontal lengths are scaled by L, vertical lengths by H, yielding the non-dimensional co-ordinates x, y, z. Horizontal velocities are scaled by U_0, as defined in § 1, and the vertical velocity by $U_0 \delta$, yielding the non-dimensional velocity vector in the ith layer $\mathbf{q}_i = (u_i, v_i, w_i)$, $i = 1, 2$ for lower and upper layer, respectively. Far from the bump, the velocity vectors are $\mathbf{q}_i = (U_i, 0, 0)$. Non-dimensional dynamic pressures p_1 and p_2 are introduced by

$$\left.\begin{aligned} p_2 &= [P_2 - \rho_2 gH(1-z)]/(\rho_0 U_0 f_0 L), \\ p_1 &= [P_1 - \rho_2 gH(1-d) - \rho_1 gH(d-z)]/(\rho_0 U_0 f_0 L). \end{aligned}\right\} \tag{2.1}$$

In terms of these variables, and the parameters introduced in § 1, the equations of motion are

$$\left.\begin{aligned} \epsilon\mathbf{q}_i . \nabla u_i - (1 + \epsilon by) v_i &= -(p_i)_x + \delta^2 E_h \nabla_h^2 u_i + E_v(u_i)_{zz}, \\ \epsilon\mathbf{q}_i . \nabla v_i + (1 + \epsilon by) u_i &= -(p_i)_y + \delta^2 E_h \nabla_h^2 v_i + E_v(v_i)_{zz}, \\ \epsilon\delta^2\mathbf{q}_i . \nabla w_i &= -(p_i)_z + \delta^4 E_h \nabla_h^2 w_i + \delta^2 E_v(w_i)_{zz}, \end{aligned}\right\} \tag{2.2}$$

$$\nabla . \mathbf{q}_i = 0,$$

where ∇_h^2 is the horizontal Laplacian operator, and ∇ is the three-dimensional gradient operator.

The non-dimensional interface height is

$$z_{1n} = d + \eta. \tag{2.3}$$

Requiring the pressures P_1 and P_2, (2.1), to be equal at the interface gives a relation between η and the individual layer dynamic pressures:

$$\eta = -\epsilon(p_2 - p_1)/S. \tag{2.4}$$

We note, in passing, that, for the present work, S is considered to be $\geqslant O(1)$. Thus, by (2.4), $\eta \leqslant O(\epsilon)$. At the interface, the condition that the interface be a material surface relates the total vertical velocities in each layer to the interface displacements:

$$w_i = u_i(\eta)_x + v_i(\eta)_y \quad \text{at} \quad z = d + \eta. \tag{2.5}$$

We are considering the parameter range

$$E_v^{\frac{1}{2}}, E_h^{\frac{1}{2}} \ll \epsilon \ll 1, \quad b \leqslant O(1), \quad \delta \leqslant O(1), \quad S = O(1).$$

For this range, the viscous terms in (2.2) can be dropped, and the dependent variables expanded in power series in the Rossby number ϵ, e.g.

$$u_i = u_i^{(0)} + \epsilon^1 u_i^{(1)} + \epsilon^2 u_i^{(2)} + \dots,$$

giving the sequence of equations: order ϵ^0,

$$\left.\begin{array}{l} v_i^{(0)} = (p_i^{(0)})_x, \quad u_i^{(0)} = -(p_i^{(0)})_y, \quad 0 = (p_i^{(0)})_z, \\ \quad (u_i^{(0)})_x + (v_i^{(0)})_y + (w_i^{(0)})_z = 0; \end{array}\right\} \tag{2.6}$$

order ϵ^1,

$$\left.\begin{array}{l} \mathbf{q}_i^{(0)} \cdot \nabla u_i^{(0)} - v_i^{(1)} - byv_i^{(0)} = -(p_i^{(1)})_x, \\ \mathbf{q}_i^{(0)} \cdot \nabla v_i^{(0)} + u_i^{(1)} + byu_i^{(0)} = -(p_i^{(1)})_y, \\ \delta^2 \mathbf{q}_i^{(0)} \cdot \nabla w_i^{(0)} \qquad\qquad = -(p_i^{(1)})_z, \\ (u_i^{(1)})_x + (v_i^{(1)})_y + (w_i^{(1)})_z = 0. \end{array}\right\} \tag{2.7}$$

Equation (2.6) implies that the lowest-order velocities in each layer are independent of the vertical co-ordinate:

$$(u_i^{(0)})_z = (v_i^{(0)})_z = (w_i^{(0)})_z = 0. \tag{2.8}$$

Hence $w^{(0)}$ is zero (for $h = O(\epsilon)$), and $p_i^{(0)}$ is the stream function for the order-ϵ^0 horizontal velocity field.

From (2.7) and (2.8), an equation for the lowest-order vorticity $\zeta_i^{(0)}$ can be derived:

$$\mathbf{q}_i^{(0)} \cdot \nabla[\zeta_i^{(0)} + by] = (w_i^{(1)})_z, \quad \zeta_i^{(0)} = \nabla_h^2 p_i^{(0)}. \tag{2.9}$$

At the top and bottom,

$$\left.\begin{array}{ll} w_1^{(1)} = u_1^{(0)}(h/\epsilon)_x + v_1^{(0)}(h/\epsilon)_y & \text{at} \quad z = h, \\ w_2^{(1)} = 0 & \text{at} \quad z = 1, \end{array}\right\} \tag{2.10}$$

where h/ϵ is assumed to be an $O(1)$ quantity. The vertical velocities at the interface are given by (2.5), which, to this order, is applied at $z = d$, since η is, by (2.4) with $S \geqslant O(1)$, an order-ϵ quantity. Since $q_i^{(0)}$ and $\zeta_i^{(0)}$ are independent of z, (2.9) shows that $(w_i^{(1)})_z$ is independent of z. Using the top, bottom, and interface vertical velocities ((2.10) and (2.4)), we obtain

$$\left.\begin{array}{l} (w_1^{(1)})_z = -\mathbf{q}_1^{(0)} \cdot \nabla\left[\dfrac{h}{d\epsilon} - \dfrac{\eta^{(1)}}{d}\right], \\[2mm] (w_2^{(1)})_z = -\mathbf{q}_2^{(0)} \cdot \nabla\left[\dfrac{\eta^{(1)}}{1-d}\right]. \end{array}\right\} \tag{2.11}$$

Hence (2.11) become, dropping superscripts (0),

$$\left.\begin{array}{l} \mathbf{q}_1 \cdot \nabla\left[\nabla_h^2 p_1 + by + \dfrac{h}{d\epsilon} - \dfrac{\eta^{(1)}}{d}\right] = 0, \\[2mm] \mathbf{q}_2 \cdot \nabla\left[\nabla_h^2 p_2 + by + \dfrac{\eta^{(1)}}{1-d}\right] = 0, \\[2mm] \qquad\qquad \eta^{(1)} = (p_1 - p_2)/S. \end{array}\right\} \tag{2.12}$$

The first two of (2.12) imply that the bracketed quantities are functions of the stream functions p_1 and p_2 alone, respectively. Letting the approaching flows be

$$p_i \to p_{i,\infty} = -U_i y, \tag{2.13}$$

noting that $dU_1^2 + (1-d)U_2^2 = 1$, and letting

$$p_i = p_{i,\infty} + \phi_i, \quad \eta^{(1)} = [(U_2 - U_1)y/S + \xi], \tag{2.14}$$

the following equations for ϕ_i and ξ are obtained from (2.12):

$$\nabla_h^2 \phi_1 - \phi_1 \left[-\frac{b}{U_1} + \frac{U_2}{U_1}\frac{1}{dS} - \frac{1}{dS} \right] = \frac{\xi}{d} - \frac{h}{d\epsilon},$$

$$\nabla_h^2 \phi_2 - \phi_2 \left[-\frac{b}{U_2} + \frac{U_1}{U_2}\frac{1}{(1-d)S} - \frac{1}{(1-d)S} \right] = \frac{\xi}{(1-d)}, \tag{2.15}$$

$$\xi = (\phi_1 - \phi_2)/S.$$

Elimination of ξ gives

$$\nabla_h^2 \phi_1 - \phi_1 \left[-\frac{b}{U_1} + \frac{U_2}{U_1}\frac{1}{dS} \right] = -\frac{\phi_2}{dS} - \frac{h}{d\epsilon},$$

$$\nabla_h^2 \phi_2 - \phi_2 \left[-\frac{b}{U_2} + \frac{U_1}{U_2}\frac{1}{(1-d)S} \right] = -\frac{\phi_1}{(1-d)S}. \tag{2.16}$$

Equations (2.16) are two coupled second-order linear partial differential equations for ϕ_1 and ϕ_2. Elimination of ϕ_1 gives a single fourth-order equation for ϕ_2:

$$\left[\nabla_h^2 + \frac{b}{U_1} - \frac{U_2}{U_1}\frac{1}{dS} \right]\left[\nabla_h^2 + \frac{b}{U_2} - \frac{U_2}{U_1}\frac{1}{(1-d)S} \right]\phi_2 - \frac{\phi_2}{d(1-d)S^2} = \frac{h}{d(1-d)\epsilon S}. \tag{2.17}$$

Equation (2.17) is to be solved for a specified function $h(r,\theta)$ and subject to the boundary conditions

$$\phi_2 \quad \text{bounded everywhere}, \quad \phi_2 \to 0 \quad \text{far from bump}. \tag{2.18}$$

For some ranges of values of the parameters b, S, d, U_1 and U_2, (2.17) assumes a wavelike character; and (2.18) are insufficient to determine a solution uniquely. When this occurs, a condition must be added of the form

$$r^{\frac12}\phi_2 \to 0 \quad \text{'upstream'}. \tag{2.19}$$

What is 'upstream' is determined by considering the linearized time-dependent equations analogous to (2.12), and calculating the phase velocity and group velocity of plane wave solutions. Requiring stationarity gives the group velocity corresponding to the wavy solutions of (2.15). The 'upstream' in (2.18) is the direction opposite to the group velocity direction for the wave. This will be discussed in more detail in §3.

To simplify notation, introduce the quantities

$$N_1 = -\frac{b}{U_1} + \frac{U_2}{U_1}\frac{1}{dS}, \quad N_2 = -\frac{b}{U_2} + \frac{U_1}{U_2}\frac{1}{(1-d)S}, \quad N_3 = \frac{1}{d(1-d)S^2}. \tag{2.20}$$

Then (2.19) becomes

$$\nabla^4 \phi_2 - (N_1 + N_2)\nabla^2 \phi_2 + (N_1 N_2 - N_3)\phi_2 = \frac{1}{d(1-d)S}\frac{h}{\epsilon}. \tag{2.21}$$

Attention will be restricted to the right circular cylindrical bump

$$h = \begin{cases} h_0 & (r < 1), \\ 0 & (r > 1). \end{cases} \qquad (2.22)$$

The generalization to more complex bumps is direct, but yields no additional phenomenon of interest.

Anticipating that closed streamlines may occur in the flow field for sufficiently large values of h_0/ϵ, the steps from (2.12) to (2.15) then break down, since the streamlines within the outermost closed streamline no longer originate upstream. Ingersoll (1969) argued that the ultimate state of an f-plane Taylor column must be stagnation (i.e. the Ekman suction term, however small, eventually kills off the interior motion, making the closed streamline defining the Taylor column a zero velocity line: $\nabla p_i = 0$). In the examples of solutions to (2.21) that are to be given here, it will not be possible to apply such a boundary condition. Indeed, for most oceanic and atmospheric situations, such solutions would correspond to very long times, and fail to be of much interest. For times short compared with the viscous time scale, the effects of viscosity should be negligible, and solutions to (2.21) should be indicative of those that would be obtained by solving the initial-value problem corresponding to the time-dependent analogues of (2.12).

3. Discussion of the general solution

The solution to the problem defined by (2.21), (2.22), (2.18) and (2.19) is obtained as follows. The domain is divided into two regions: $r < 1$ and $r > 1$. In each region ϕ_2 is expressed as a Fourier series in θ. The nth equation thus obtained has four homogeneous solutions: $P_n(k_1 r)$, $Q_n(k_1 r)$, $P_n(k_2 r)$ and $Q_n(k_2 r)$. P_n is a Bessel function of the first kind, nth order (ordinary if argument is real, hyperbolic if argument is imaginary). Q_n is the corresponding Bessel function of the second kind. The constants k_1 and k_2 are given by

$$\begin{aligned} k_1^2 &= -\tfrac{1}{2}(N_1 + N_2) + \tfrac{1}{2}[(N_1 - N_2)^2 + 4N_3]^{\frac{1}{2}}, \\ k_2^2 &= -\tfrac{1}{2}(N_1 + N_2) - \tfrac{1}{2}[(N_1 - N_2)^2 + 4N_3]^{\frac{1}{2}}. \end{aligned} \qquad (3.1)$$

There are four distinct cases determined by the magnitudes and signs of N_1, N_2 and N_3. These are summarized in table 2. By definition,

$$\begin{aligned} N_1 + N_2 &= \frac{1}{U_1 U_2}\left[-(U_1 + U_2)b + \frac{1}{d(1-d)S} \right], \\ N_1 N_2 - N_3 &= \frac{b}{U_1 U_2}\left[b - \frac{dU_1 + (1-d)U_2}{d(1-d)S} \right]. \end{aligned} \qquad (3.2)$$

Thus case (i) includes all those situations with both currents retrograde ($U_1 < 0$ and $U_2 < 0$).

When both currents are prograde, there will always be at least one wavy mode. This is easily seen from (3.2). To get case (i) would require

$$U_1 + U_2 < \frac{1}{bd(1-d)S} < \frac{1}{dU_1 + (1-d)U_2}.$$

Case	$N_1 + N_2$	$N_1 N_2 - N_3$	k_1^2	k_2^2
(i) Two evanescent	> 0	> 0	< 0	< 0
(ii) Two wavy	< 0	> 0	> 0	> 0
(iii) One evanescent, one wavy	> 0	< 0	> 0	< 0
(iv) One evanescent, one wavy	< 0	< 0	> 0	< 0

TABLE 2. Summary of character of fundamental solutions for different values of $N_1 + N_2$ and of $N_1 N_2 - N_3$

U_1	U_2	$U_1 + U_2$	$dU_1 + (1-d) U_2$	Cases occurring
< 0	< 0	< 0	< 0	(i)
> 0	> 0	> 0	> 0	(ii), (iii) or (iv)
< 0	> 0	> 0	> 0	(ii), (iii) or (iv)
		> 0	< 0	(iii) or (iv)
		< 0	< 0	(iv)
> 0	< 0	> 0	> 0	(ii), (iii) or (iv)
		< 0	> 0	(ii) or (iv)
		< 0	< 0	(iv)

TABLE 3. Summary of different cases occurring for different values of the two layer velocities

or, since $dU_1^2 + (1-d) U_2^3 = 1$,

$$U_1 U_2 < 0.$$

This is impossible for $U_1 > 0$, $U_2 > 0$. If all quantities except b are fixed, and both velocities are prograde, then, as b is increased from zero (by varying U_0), the sequence of cases is (iii), (iv), (ii). If all quantities except S are fixed, and both velocities are prograde, then, as S is increased, the same sequence of cases occurs.

When the lower layer is retrograde and the upper prograde, or vice versa, there will always be at least one wavy mode. Which cases occur depends on the signs of the velocity sum, $U_1 + U_2$, and the volume flux, $dU_1 + (1-d) U_2$. The various possibilities are summarized in table 3 for the situation $d > 0.5$.

The determination of the appropriate 'upstream' condition for a wavy mode goes as follows. Plane wave solutions (form $C \exp[i\alpha_i x - i\omega_i t]$) of the time-dependent linearized equations analogous to (2.12) are examined. The equation for α_i and ω_i thus obtained is

$$\omega_i^2 \alpha_i^2 + \omega_i \alpha_i [U_1 N_1 + U_2 N_2 + \alpha_i^2 (U_1 + U_2)]$$
$$+ U_1 U_2 [(N_1 + \alpha_i^2)(N_2 + \alpha_i^2) - N_3] = 0. \qquad (3.3)$$

Stationarity, $\omega_i = 0$, gives $\alpha_i^2 = k_i^2$, where the k_i^2 are given by (3.1). Differentiation of (3.3) with respect to α_i gives an equation for the corresponding group velocity $c_{g,i} = \partial \omega_i / \partial \alpha_i$. When $\omega_i = 0$ and $\alpha_i^2 = k_i^2$ are substituted, this is

$$c_{g,i} = 4U_1 U_2 \left\{ U_2 \left(1 \mp \frac{N_1 - N_2}{[(N_1 - N_2)^2 + 4N_3]^{\frac{1}{2}}}\right) + U_1 \left(1 \pm \frac{N_1 - N_2}{[(N_1 - N_2)^2 + 4N_3]^{\frac{1}{2}}}\right) \right\}^{-1}, \qquad (3.4)$$

where upper signs correspond to k_1^2 and lower signs to k_2^2.

When both velocities are prograde, $c_{g,i}$ is always greater than zero. Hence 'upstream' is to the west, as in the homogeneous case. When one of the counter-flow situations occurs, $c_{g,i}$ will be positive only if

$$U_2\left(1 \mp \frac{N_1 - N_2}{[(N_1 - N_2)^2 + 4N_3]^{\frac{1}{2}}}\right) + U_1\left(1 \pm \frac{N_1 - N_2}{[(N_1 - N_2)^2 + 4N_3]^{\frac{1}{2}}}\right) < 0. \tag{3.5}$$

There will be situations in which (3.5) is violated. Hence the counter-flow situations must be evaluated individually.

The pure retrograde and pure prograde situations will be discussed in §§ 4 and 5. The possibility of baroclinic instability, either of the basic approaching flow, or induced by the interaction with the bump, will not be considered here. For the basic flow field considered here, Pedlosky (1964, (3.2.9)) showed that the necessary and sufficient condition for stability is the following constraint on the vertical shear (in the present notation):

$$U_2 - U_1 < bdS. \tag{3.6}$$

The right-hand side of (3.6) is independent of the horizontal length scale L. No attempt to force the parameters of the specific examples in the following sections to satisfy (3.6) will be made. Nor will any attempt be made to determine whether interaction with the bump will cause instabilities.

4. Solutions for two retrograde currents

In §3 we found that, when both currents are retrograde, the fundamental solutions to (2.21) are evanescent in character. The solution for ϕ_2 is in this case independent of θ (polar co-ordinates), and is

$$\phi_2 = \frac{h_0}{d(1-d)\epsilon S}\begin{cases} A_0 I_0[|k_1^2|^{\frac{1}{2}}r] + B_0 I_0[|k_2^2|^{\frac{1}{2}}r] + F_0 & (r < 1), \\ C_0 K_0[|k_1^2|^{\frac{1}{2}}r] + D_0 K_0[|k_2^2|^{\frac{1}{2}}r] & (r > 1), \end{cases} \tag{4.1}$$

with k_1^2 and k_2^2 given by (3.1), and where

$$F_0 = [N_1 N_2 - N_3]^{-1} \tag{4.2}$$

is the particular integral of the governing equation (2.21) corresponding to the height distribution (2.22). The other constants (A_0, B_0, C_0 and D_0) are obtained by requiring that ϕ_2 and its first three radial derivatives be continuous at $r = 1$. The expressions for the constants are very complicated, and will not be given here.

From ϕ_2, ϕ_1 and ξ are computed from the second of (2.16) and the third of (2.15), respectively:

$$\phi_1 = \frac{h_0}{d\epsilon}\begin{cases} A_0[N_2 + k_1^2] I_0[|k_1^2|^{\frac{1}{2}}r] + B_0[N_2 + k_2^2] I_0[|k_2^2|^{\frac{1}{2}}r] + N_2 F_0 & (r < 1), \\ C_0[N_2 + k_1^2] K_0[|k_1^2|^{\frac{1}{2}}r]D_0 + [N_2 + k_2^2] K_0[|k_2^2|^{\frac{1}{2}}r] & (r > 1), \end{cases}$$

$$\xi = \frac{h_0}{d\epsilon}\begin{cases} A_0\left[N_2 + k_1^2 - \dfrac{1}{(1-d)S}\right] I_0[|k_1^2|^{\frac{1}{2}}r] + \left[N_2 - \dfrac{1}{(1-d)S}\right] F_0 \\ \qquad\qquad + B_0\left[N_2 + k_2^2 - \dfrac{1}{(1-d)S}\right] I_0[|k_2^2|^{\frac{1}{2}}r] \quad (r < 1), \\ C_0\left[N_2 + k_1^2 - \dfrac{1}{(1-d)S}\right] K_0[|k_1^2|^{\frac{1}{2}}r] \\ \qquad\qquad + D_0\left[N_2 + k_2^2 - \dfrac{1}{(1-d)S}\right] K_0[|k_2^2|^{\frac{1}{2}}r] \quad (r > 1). \end{cases} \tag{4.3}$$
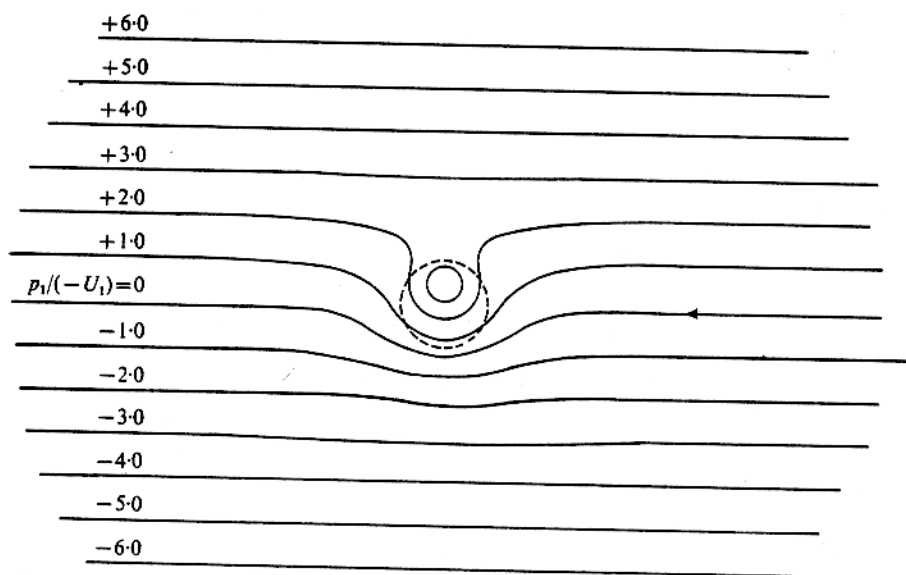
FIGURE 2. Lower-layer streamlines for retrograde (westward) flow past a right circular cylindrical bump (----). $|b/U_1| = 1.0$, $S \to \infty$, $h_0/(d\epsilon) = 6.0$. Lower layer behaves as though it were a single layer, with a rigid lid at $z = d$.

The actual interface displacement η is given by

$$\eta = \epsilon[y(U_2 - U_1)/S + \xi], \qquad (4.4)$$

and for $U_1 < 0$ and $U_2 < 0$, $k_1^2 < 0$ and $k_2^2 < 0$.

The character of these solutions is clarified by considering two limiting cases. First, let $S \to \infty$. Then

$$N_1 \to -b/U_1, \quad N_2 \to -b/U_2, \quad N_3 \to 0.$$

Hence
$$k_2^2 \to +b/U_2, \quad k_1^2 \to +b/U_1 \quad (U_1 < 0, U_2 < 0).$$

Thus
$$\phi_2 \to 0, \quad \xi \to 0,$$

$$\phi_1 \to \frac{h_0}{d\epsilon}\begin{cases} A_0' I_0[(-b/U_1)^{\frac{1}{2}}r] + F_0' & (r < 1), \\ C_0' K_0[(-b/U_1)^{\frac{1}{2}}r] & (r > 1), \end{cases} \qquad (4.5)$$

where
$$A_0' = -(-U_1/b)^{\frac{1}{2}} K_1 (-U_1/b)^{\frac{1}{2}},$$

$$C_0' = +(-U_1/b)^{\frac{1}{2}} I_1 (-U_1/b)^{\frac{1}{2}} \quad \text{and} \quad F_0' = (-U_1/b).$$

The lower layer behaves as though the interface is a rigid lid. Thus the expression for ϕ_1 in (4.5) is identical to that which would result from solving the equations corresponding to a single homogeneous layer of thickness d and approaching flow velocity U_1.

Ingersoll's (1969) f-plane, homogeneous fluid result can be obtained from (4.5) by letting $-b/U_1 \to 0$, and restricting the arguments of the Bessel functions: $(-b/U_1)^{\frac{1}{2}}r \ll 1$. This gives

$$\phi_2 = -\frac{h_0}{2d\epsilon}\begin{cases} \ln(r) + \text{const.} & (r > 1), \\ \frac{1}{2}r^2 + \text{const.} & (r < 1). \end{cases} \qquad (4.6a)$$
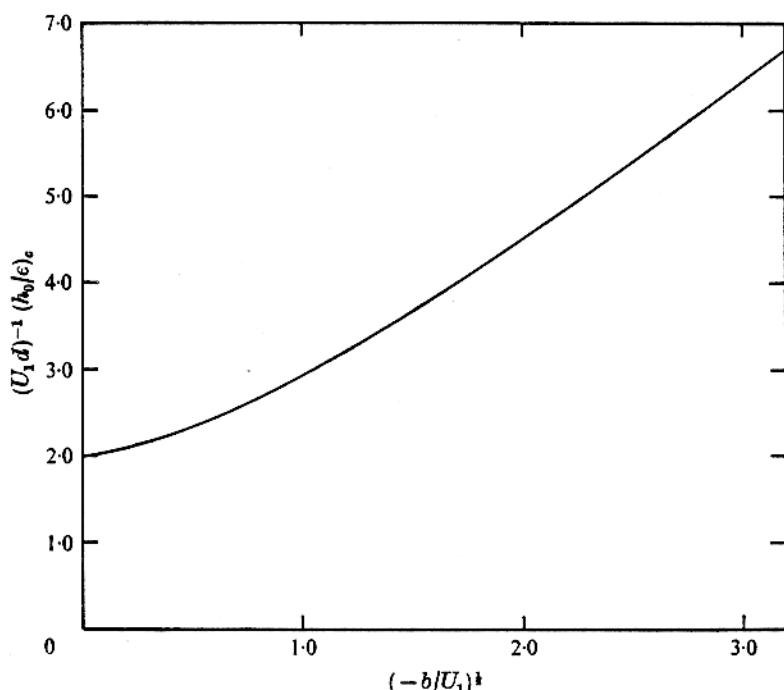
FIGURE 3. Minimum obstacle height giving a Taylor column in the lower layer for the limit $S \to \infty$, for a right circular cylindrical bump.

But, for r sufficiently large, $(-b/U_1)^{\frac{1}{2}} r \gg 1$, and

$$\phi_2 \to \frac{h_0}{2d\epsilon} (\tfrac{1}{2}\pi)^{\frac{1}{2}} (-U_1/b)^{\frac{1}{4}} \frac{\exp\left[-(-U_1/b)^{\frac{1}{2}}r\right]}{r^{\frac{1}{2}}} \quad (r \gg 1), \qquad (4.6b)$$

indicating an exponentially decaying disturbance. Thus, whereas the natural logarithm in Ingersoll's solution, $(4.6a)$, implies that streamlines climb to larger and larger values of y as r increases, $(4.6b)$ shows that eventually β comes into play and limits the radial extent of the disturbance. This is evident in figure 2, where streamlines corresponding to the $S \to \infty$ solution, (4.5), with $(-b/U_1) = 1 \cdot 0$, $h_0/(d\epsilon) = 6 \cdot 0$ are shown. The flow deflects to the left (to the right in southern hemisphere) and accelerates as it passes the bump, with maximum velocities of the order of $3U_1$. The associated (anti-cyclonic) circulation Γ_1 is

$$\Gamma_1 = \int_0^{2\pi} \frac{\partial \phi_1}{\partial r}\bigg|_{r=1} d\theta = -\frac{2\pi h_0}{d\epsilon} I_1(-b/U_1)^{\frac{1}{2}}) K_1((-b/U_1)^{\frac{1}{2}}), \qquad (4.7)$$

which, for $b \ll 1$, gives $\Gamma_1 \approx -\pi h_0/\epsilon$ (i.e. Ingersoll's (1969) result). For $b \gg 1$, it gives $\Gamma_1 \to -\pi h_0/(\epsilon(-b/U_1)^{\frac{1}{2}})$. In the figure, the Taylor column is well developed. The value of h_0 necessary to force a Taylor column $(h_0)_c$ is easily found from (4.5) by looking for the minimum value that gives a stagnation point, $\nabla p_1 = 0$. The calculation gives

$$(h_0/\epsilon)_c = U_1 d/I_1((-b/U_1)^{\frac{1}{2}}) K_1((-b/U_1)^{\frac{1}{2}}). \qquad (4.8)$$

This function is plotted in figure 3. For $b \ll 1$, $(h_0/\epsilon)_c = 2d$, while, for $b \gg 1$, $(h_0/\epsilon)_c = 2(-b/U_1)^{\frac{1}{2}} d$.

6

The last limiting case is when the two velocities are equal: $U_1 = U_2 = -1$. Then

$$k_1^2 = -b, \quad k_2^2 = -b - (d(1-d)S)^{-1}.$$

ϕ_2 is given by (4.1), while ϕ_1 and ξ are

$$\phi_1 = \frac{h_0}{d\epsilon} \begin{cases} A_0 \left[\dfrac{1}{(1-d)S}\right] I_0[(-k_1^2)^{\frac{1}{2}} r] + \left[b + \dfrac{1}{(1-d)S}\right] F_0 \\ \qquad\qquad\qquad - B_0 \left[\dfrac{1}{dS}\right] I_0[(-k_2^2)^{\frac{1}{2}} r] \quad (r < 1), \\ C_0 \left[\dfrac{1}{(1-d)S}\right] K_0[(-k_1^2)^{\frac{1}{2}} r] - D_0 \left[\dfrac{1}{dS}\right] K_0[(-k_2^2)^{\frac{1}{2}} r] \qquad (r > 1); \end{cases}$$

$$\xi = \frac{h_0}{d\epsilon} \begin{cases} -B_0 \left[\dfrac{1}{d(1-d)S}\right] I_0[(-k_2^2)^{\frac{1}{2}} r] + bF_0 \quad (r < 1), \\ -D_0 \left[\dfrac{1}{d(1-d)S}\right] K_0[(-k_2^2)^{\frac{1}{2}} r], \qquad (r > 1). \end{cases} \qquad (4.9)$$

Thus the k_1 mode is, in this case, barotropic in nature (i.e. it has the same magnitude in each layer). The contributions to ϕ_1 and ϕ_2 by the k_2 mode are of opposite sign, and unequal magnitude.

The streamlines for the general case ((4.1) and (4.3)) are similar in character to those shown in figure 2 for the special case $S \to \infty$. In general, stratification attenuates the disturbance due to the bump in the upper layer. Hogg (1973) obtained a similar result for a linearly-stratified f-plane system. The limiting cases described above show that the k_1 mode is in general a modification of the solution for a single layer of homogeneous fluid. The k_2 mode reflects the system's stratification, and vanishes when the fluid is homogeneous.

5. Solutions for two prograde currents

We recall from table 3 that, when both U_1 and U_2 are greater than zero, there can be either one wavy and one evanescent solution or two wavy solutions. Also, we found in § 3 that the appropriate additional boundary condition for the wavy solution(s) was no waves upstream (to the west):

$$r^{\frac{1}{2}} \phi_2 \to 0 \quad \text{at} \quad x \to -\infty. \qquad (5.1)$$

We shall present the solution corresponding to case (iii) (i.e. $k_1^2 > 0$ and $k_2^2 < 0$). The solution is obtained by the same procedure as was used in § 4. The boundary condition indicated in (5.1) is applied as follows. In the Fourier series representation of ϕ_2, the asymptotic expressions for the various Bessel functions are introduced. The condition in (5.1) then implies that certain infinite sums of coefficients and trigonometric functions vanish for $\frac{1}{2}\pi < \theta < \frac{3}{2}\pi$. Fourier series theory is then used to obtain unique values for the coefficients involved. The details are similar to (although somewhat simpler than) the construction of lee wave functions described by Miles & Huppert (1968). They are described in McCartney (1972).

The solution thus obtained is

$$\phi_2 = \frac{4}{\pi} C_0 \frac{h_0}{d(1-d)\,\epsilon S} \Sigma + \frac{h_0}{d(1-d)\,\epsilon S} \begin{cases} A_0 J_0[k_1 r] + B_0 I_0[(-k_2^2)^{\frac{1}{2}} r] + F_0 & (r < 1), \\ C_0 Y_0[k_1 r] + D_0 K_0[(-k_2^2)^{\frac{1}{2}} r] & (r > 1), \end{cases}$$

(5.2)

where

$$\Sigma = \sum_{n=1}^{\infty} \frac{J_{2n-1}[k_1 r] \cos[(2n-1)\theta]}{2n-1},$$

with $F_0 = 1/[N_1 N_2 - N_3]$, and A_0, B_0, C_0 and D_0 constants determined by matching at $r = 1$, as in § 4.

To obtain ϕ_1 and ξ, we use the second of (2.16) and the third of (2.15), respectively, giving

$$\left. \begin{aligned} \phi_1 &= \frac{4}{\pi} C_0 \frac{h_0}{d\epsilon} [N_2 + k_1^2] \Sigma \\ &\quad + \frac{h_0}{d\epsilon} \begin{cases} A_0[N_2 + k_1^2] J_0[k_1 r] + B_0[N_2 + k_2^2] I_0[(-k_2^2)^{\frac{1}{2}} r] + N_2 F_0 & (r < 1), \\ C_0[N_2 + k_1^2] Y_0[k_1 r] + D_0[N_2 + k_2^2] K_0[(-k_2^2)^{\frac{1}{2}} r] & (r > 1), \end{cases} \\ \xi &= \frac{4}{\pi} C_0 \frac{h_0}{d\epsilon} \left[N_2 + k_1^2 - \frac{1}{(1-d)S} \right] \Sigma \\ &\quad + \frac{h_0}{d\epsilon} \begin{cases} A_0 \left[N_2 + k_1^2 - \frac{1}{(1-d)S} \right] J_0[k_1 r] + B_0 \left[N_2 + k_2^2 - \frac{1}{(1-d)S} \right] \\ \qquad\qquad \times I_0[(-k_2^2)^{\frac{1}{2}} r] + \left[N_2 - \frac{1}{(1-d)S} \right] F_0 & (r < 1), \\ C_0 \left[N_2 + k_1^2 - \frac{1}{(1-d)S} \right] Y_0[k_1 r] + D_0 \left[N_2 + k_2^2 + \frac{1}{(1-d)S} \right] \\ \qquad\qquad \times K_0[(-k_2^2)^{\frac{1}{2}} r] & (r > 1), \end{cases} \end{aligned} \right\}$$

(5.3)

with the actual interface displacement η given by (4.4).

The limiting cases examined in § 4 can also be looked at for the present solution. For $S \to \infty$,

$$N_1 \to -b/U_1, \quad N_2 \to -b/U_2, \quad N_3 \to 0.$$

Hence

$$k_1^2 \to +b/U_1, \quad k_2^2 \to +b/U_2 \quad (U_1 > 0, U_2 > 0).$$

Thus,

$$\phi_2 \to 0, \quad \xi \to 0,$$

$$\phi_1 \to \frac{4}{\pi} C_0' \frac{h_0}{d\epsilon} \left(\sum_{n=1}^{\infty} \frac{J_{2n-1}[(b/U_1)^{\frac{1}{2}} r] \cos[(2n-1)\theta]}{2n-1} \right)$$
$$+ \frac{h_0}{d\epsilon} \begin{cases} A_0' J_0[(b/U_1)^{\frac{1}{2}} r] + F_0' & (r < 1), \\ C_0' Y_0[(b/U_1)^{\frac{1}{2}} r] & (r > 1), \end{cases}$$

(5.4)

where

$$A_0' = -\tfrac{1}{2} \pi (U_1/b)^{\frac{1}{2}} Y_1(U_1/b)^{\frac{1}{2}}, \quad C_0' = -\tfrac{1}{2} \pi (U_1/b)^{\frac{1}{2}} J_1(U_1/b)^{\frac{1}{2}}, \quad F_0' = -(U_1/b).$$

As in the same limit in § 4, the interface acts as a rigid lid, and the ϕ_1 solution in (5.4) is identical to that which would result from solving the single homogeneous layer problem. The details of Ingersoll's (1969) f-plane solution can again be recovered by taking the limit $b/U_1 \to 0$.
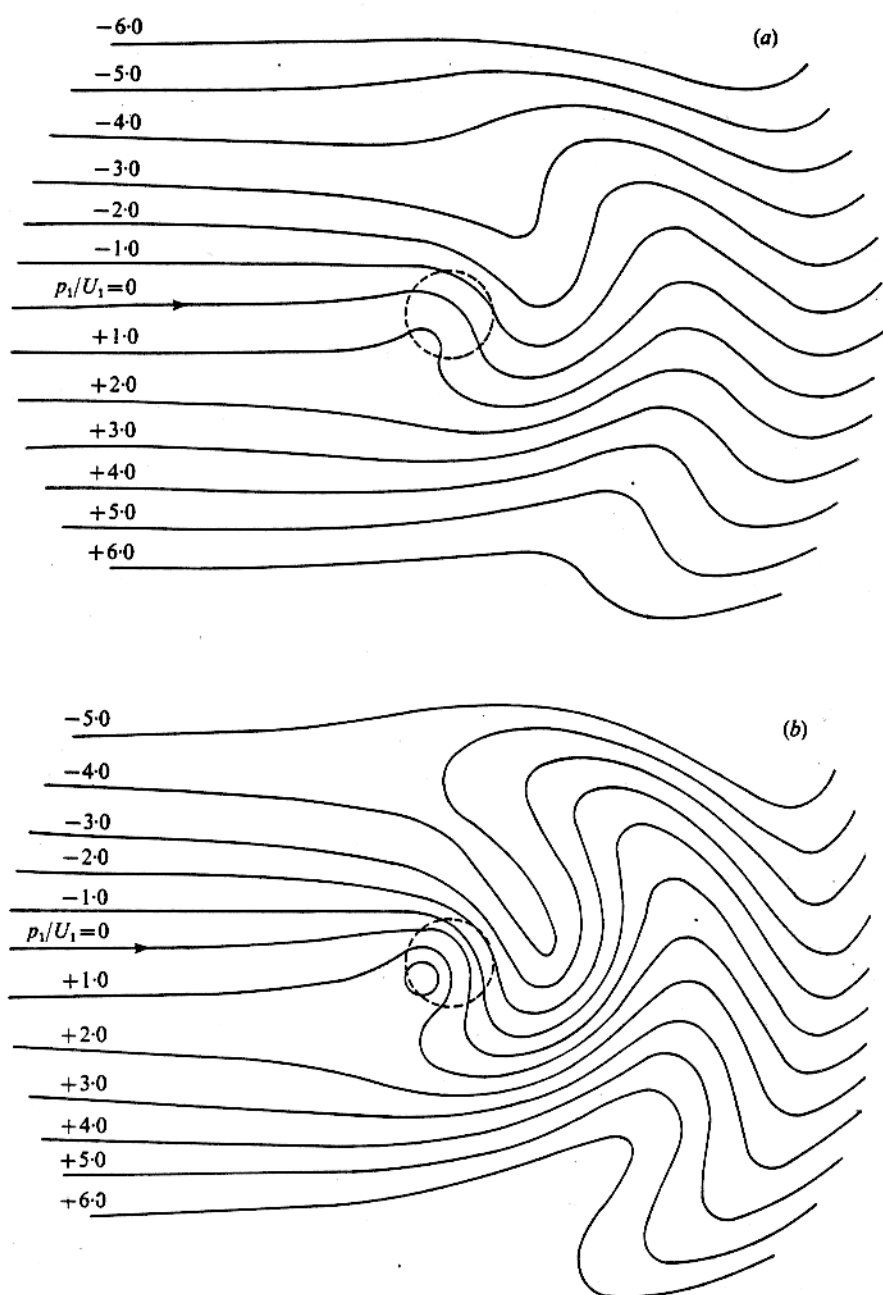
FIGURES 4(a) and (b). For legend see facing page.

The solution given in (5.4) includes a rather extensive meandering wake down-stream of the bump. In figure 4, streamlines corresponding to (5.4) with $b/U_1 = 1·0$, and three values of $h_0/(d\epsilon)$ (viz. 2·0, 4·0 and 6·0) are shown. Even for $h_0/(\epsilon d) = 2·0$ (figure 4a) the meandering wake has a north–south peak-to-peak amplitude of about 2. Over the bump, the deflexion is again to the left; but the anti-cyclonic
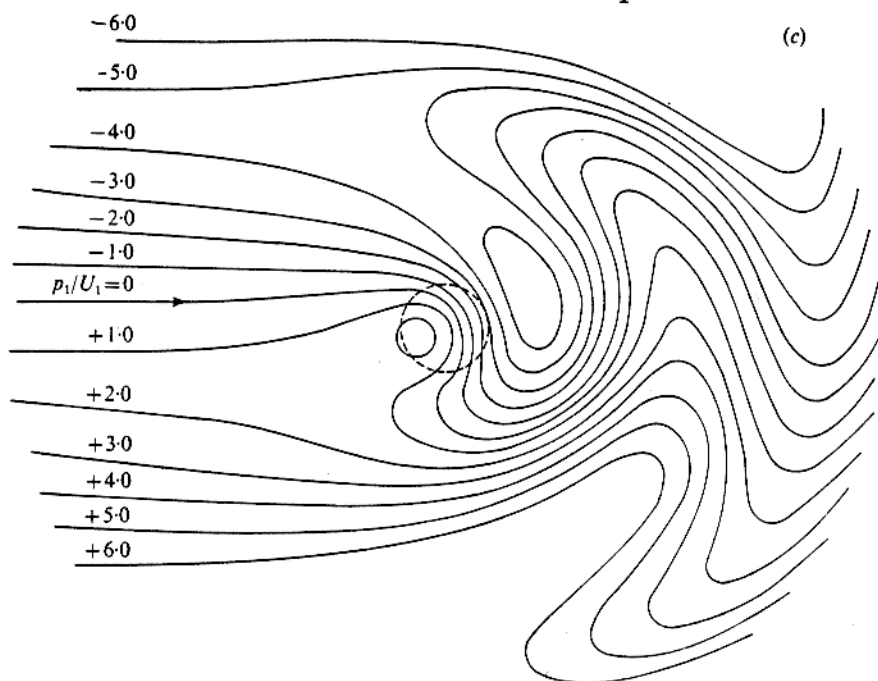
FIGURE 4. Lower-layer streamlines for prograde (eastward) flow past a right circular cylindrical bump (---). Lower layer behaves as though it were a single layer, with a rigid lid at $z = d$. $|b/U_1| = 1\cdot0$, $S \to \infty$.

|	(a)	(b)	(c)
$h_0/(d\epsilon)$	$2\cdot0$	$4\cdot0$	$6\cdot0$

Taylor column is shifted towards the front of the bump. The circulation around the bump is

$$\Gamma_1 = \int_0^{2\pi} \frac{\partial\phi_1}{\partial r}\bigg|_{r=1} d\theta = +\frac{h_0}{d\epsilon} \pi^2 J_1((b/U_1)^{\frac{1}{2}}) Y_1((b/U_1)^{\frac{1}{2}}), \tag{5.5}$$

which is negative for the example, but in general can have either sign. There is not, in general, a simple expression for the minimum height $(h_0)_c$ analogous to (4.8) for the retrograde flow. For the example, the critical value of $h_0/(d\epsilon)$ is between $2\cdot0$ and $4\cdot0$. To the east-poleward side of the bump, there is a large cyclonic loop, which, by $h_0/(d\epsilon) = 6\cdot0$, has pinched off, forming a cyclonic eddy. The anti-cyclonic meander to the east-equatorward side of the bump will also close, forming an anti-cyclonic eddy, for a still larger value of h_0. As h_0 is increased still farther, additional eddies will form in the wake. In addition to these slow regions, the wake also exhibits an alternate jet character. In figure 4(b), for example, to the east-equatorward side of the bump, at about $r = 3$, there is an east-poleward directed jet with velocities of the order of $3U_1$.

Recalling that the streamlines are constant-pressure lines, it is evident from figure 4 that there is a downstream force D on the bump: a wave drag. This is easily calculated by integrating the pressure distribution around $r = 1$. Using ϕ_1 from (5.4), we obtain a drag coefficient

$$C_D \equiv \frac{D}{\rho U_1 f_0 L^3} = 2\pi \frac{\delta\epsilon}{d} \left(\frac{h_0}{\epsilon}\right)^2 \frac{J_1^2((b/U_1)^{\frac{1}{2}})}{(b/U_1)^{\frac{1}{2}}}. \tag{5.6}$$
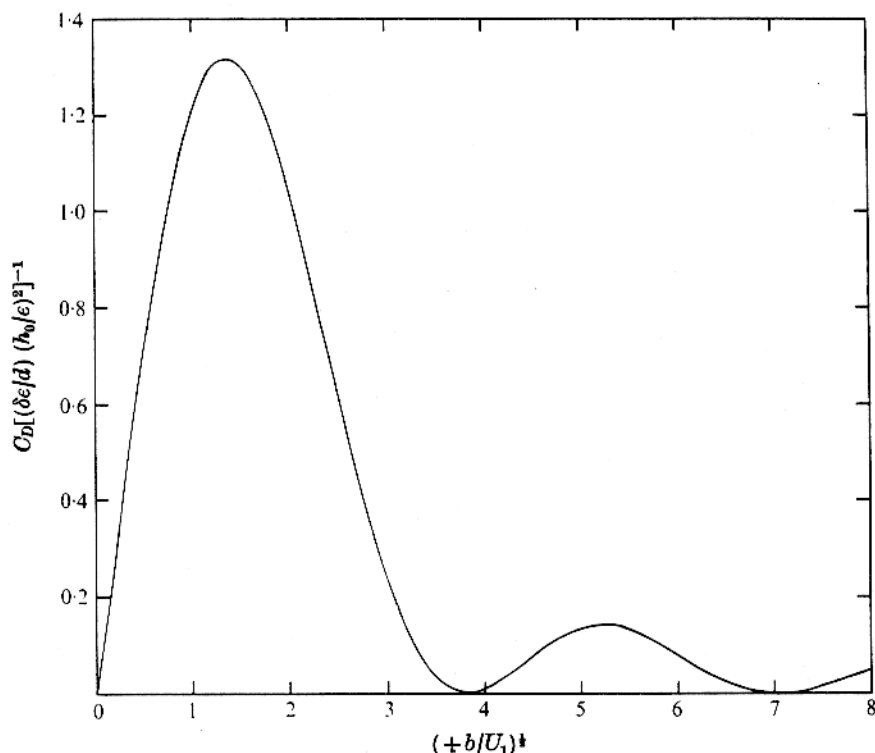
FIGURE 5. Drag coefficient for the limit $S \to \infty$.

This is plotted in figure 5, as a function of $(b/U_1)^{\frac{1}{2}}$. For comparison, the Ekman drag on a circular area of radius L on an infinite plane, with a current of magnitude U_0 flowing over it, has the drag coefficient

$$C_{D,\,\text{Ekman}} = \pi \delta E_v^{\frac{1}{2}}.$$

Of course, since we assumed $\epsilon \gg E_v^{\frac{1}{2}}$, the wave drag is thus much greater than any possible viscous drag contribution.

The wave drag vanishes at the zeros of $J_1(b/U_1)^{\frac{1}{2}}$. The streamlines corresponding to the first two zeros are shown in figure 6. We see that a resonance phenomenon is occurring: there is no disturbance outside the bump, and an integral number of waves over the bump. This occurs because of the particular $h(r)$ we used. But it can occur for more general choices of $h(r)$, when certain integrals of $h(r)$ and Bessel functions vanish. The particular values of h_0 in figure 6 are those that first give a stagnation point over the bump. The location of the point is indicated by a cross.

The second limit is when $U_1 = U_2 = +1$. The k_1 mode becomes barotropic in nature, just as in the corresponding retrograde solution limit (see discussion of (4.7)). The interface does not, for this limit, have a wavy character (i.e. in ξ the k_1 contribution is zero).
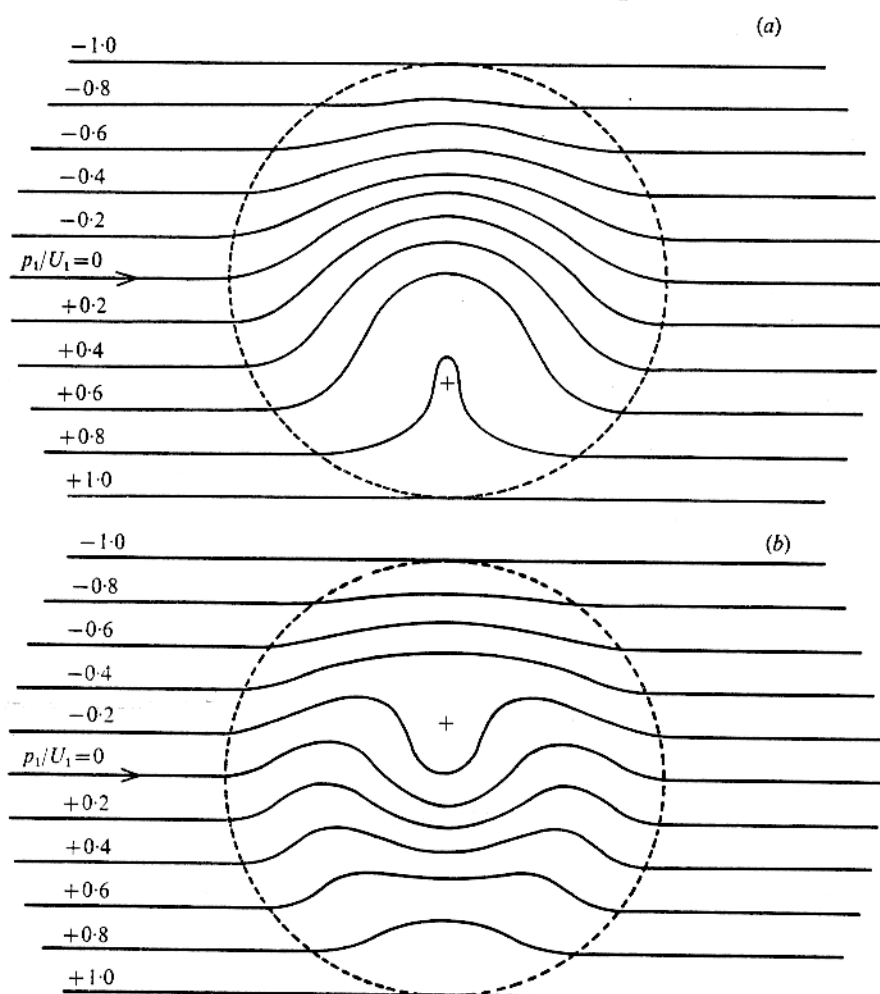
FIGURE 6. Lower-layer streamlines for prograde (eastward) flow past a right circular cylindrical bump (----), for the values of $|b/U_1|$ that correspond to the first two zeros of the Bessel function J_1, and those of $h_0/(d\epsilon)$ that just cause a stagnation point (+).
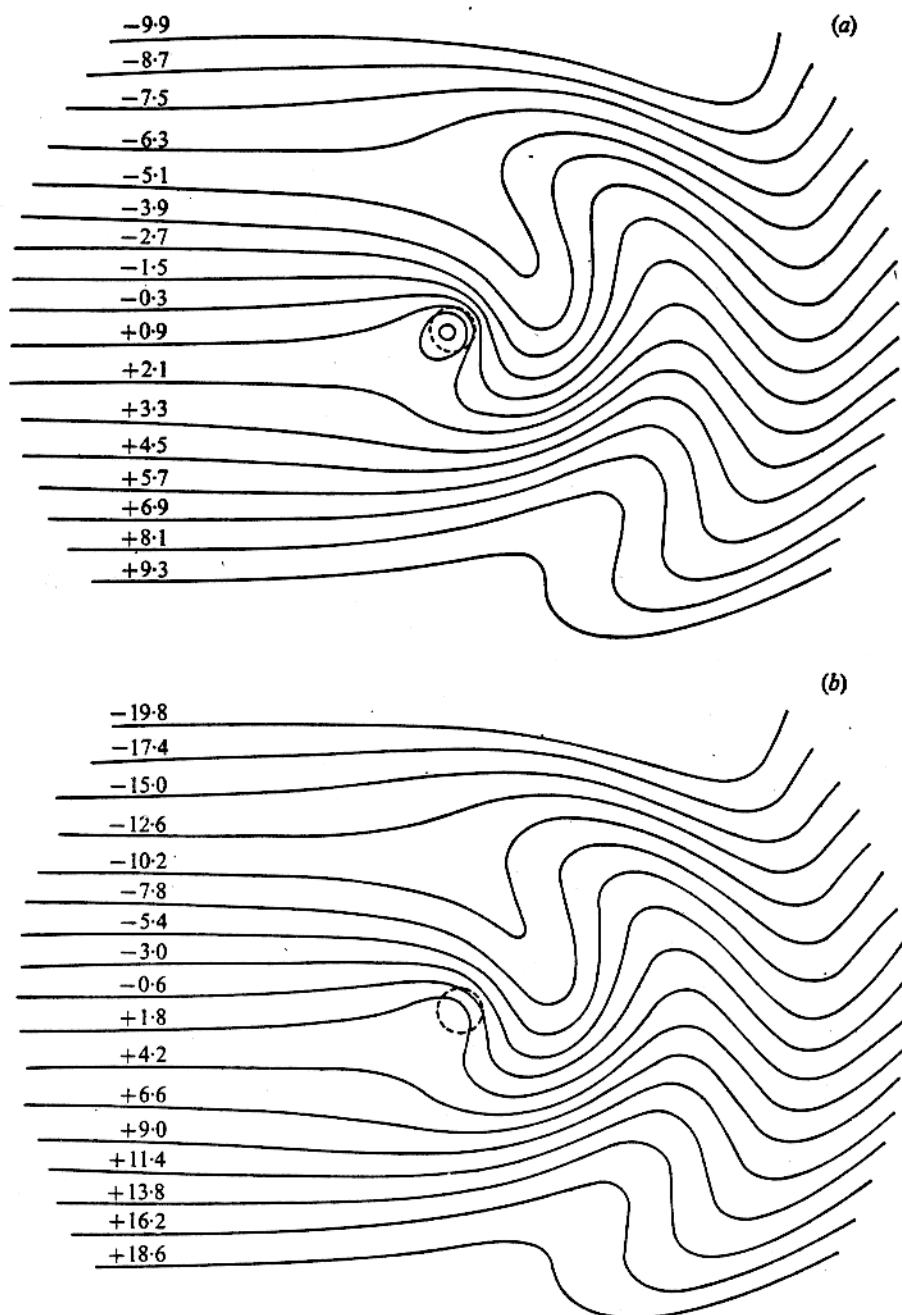
	$|b/U_1|$	$h_0/(d\epsilon)$
(a)	·14·86	2·65
(b)	49·1	3·61

Results for a specific example of the general prograde solution ((5.2) and (5.3)) are presented. The various parameters of the problem are given the values

$$H = 5 \, \text{km}, \qquad L = 50 \, \text{km}, \qquad d = 0.8,$$

$$\Delta\rho/\rho = 10^{-3}, \qquad f_0 = 10^{-4} \, \text{s}^{-1}, \qquad \beta = 1.57 \times 10^{-13} \, (\text{cm s}^{-1}),$$

$$\mathscr{U}_1 = 10 \, \text{cm s}^{-1}, \qquad \mathscr{U}_2 = 20 \, \text{cm s}^{-1}.$$

The β value corresponds to latitude 45° and a planetary radius of 6370 km. These give the dimensionless parameters

$$\epsilon = 0.0253, \quad b = 0.3099, \quad U_1 = 0.791, \quad U_2 = 1.581, \quad S = 1.96,$$

(a)

```
−9·9
−8·7
−7·5
−6·3
−5·1
−3·9
−2·7
−1·5
−0·3
+0·9
+2·1
+3·3
+4·5
+5·7
+6·9
+8·1
+9·3
```

(b)

```
−19·8
−17·4
−15·0
−12·6
−10·2
−7·8
−5·4
−3·0
−0·6
+1·8
+4·2
+6·6
+9·0
+11·4
+13·8
+16·2
+18·6
```

FIGURES 7(a) and (b). For legend see facing page.

for which $k_1 = 0\cdot5457$ and $(-k_2^2)^{\frac{1}{2}} = 1\cdot5036$. The constants in (5.2) are then

$$A_0 = +1\cdot537, \quad B_0 = +0\cdot07173, \quad C_0 = -0\cdot2957,$$
$$D_0 = -0\cdot2561, \quad F_0 = -1\cdot4856.$$

For a bump height of $760\,\text{m}$, $h_0/\varepsilon = 6\cdot0$. The streamlines and interface contours corresponding to these parameters are shown in figure 7. Comparison of the
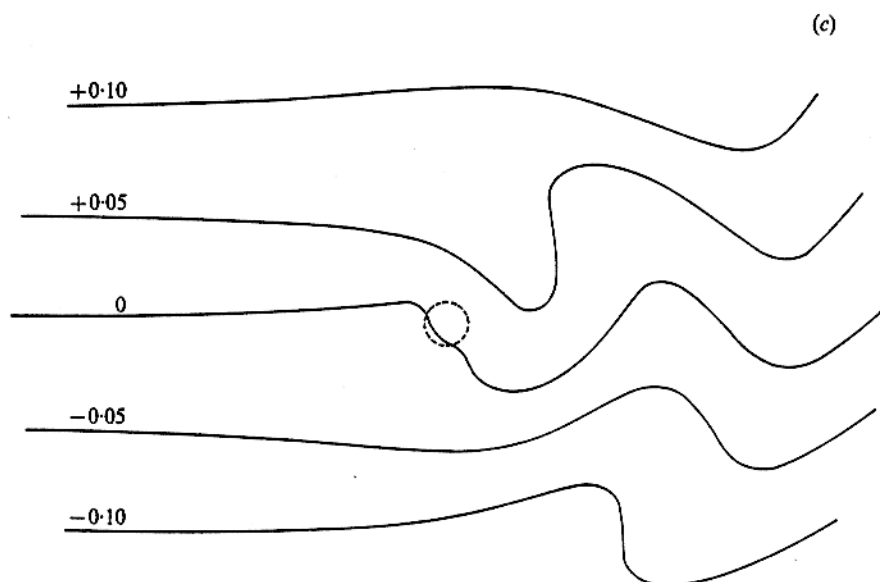
(c)

FIGURE 7. Streamlines and interface contours for $b = 0.3099$, $S = 1.96$, $U_1 = 0.791$, $U_2 = 1.581$ and $h_0/\epsilon = 6.0$. (a) Lower-layer streamlines. (b) Upper-layer streamlines. (c) Interface contours.

streamlines for the two layers shows that the disturbance over the bump is weaker in the upper layer, agreeing with Hogg's (1973) result for continuous stratification on an f plane. But, away from the bump, the meandering wake is of nearly the same amplitude in both layers. In the far wake downstream, we have (by substitution of the asymptotic forms of all the Bessel functions)

$$\left. \begin{aligned} \phi_2 &\simeq \frac{h_0}{d\epsilon} \frac{1}{(1-d)S} C_0 Y_0[k_1 r], \\ \phi_1 &\simeq \frac{h_0}{d\epsilon} 2C_0[N_2 + k_1^2] Y_0[k_1 r], \\ \xi &\simeq \frac{h_0}{d\epsilon} 2C_0 \left[N_2 + k_1^2 - \frac{1}{(1-d)S} \right] Y_0[k_1 r]. \end{aligned} \right\} \tag{5.7}$$

Thus the asymptotic ratio of lower-layer disturbance to upper-layer disturbance is

$$\phi_1/\phi_2 \simeq [N_2 + k_1^2](1-d)S. \tag{5.8}$$

For the example, this number is 0.54, or very nearly $U_1/U_2 = 0.50$, hence the asymptotic similarity of the streamlines. This near equality is due to the smallness of b; because, for $b \ll 1$, $k_1^2 \ll 1$. Hence,

$$N_2 + k_1^2 \simeq N_2 \simeq \frac{U_1}{U_2} \frac{1}{(1-d)S}, \qquad \frac{\phi_1}{\phi_2} \simeq \frac{U_1}{U_2}.$$

Retention of the lowest-order terms in b gives

$$\frac{\phi_1}{\phi_2} \simeq \frac{U_1}{U_2} \left[1 + \frac{2b(U_2 - U_1)}{SN_3} \right],$$

indicating, for $U_2 > U_1$, a ratio larger than U_1/U_2.

Returning to figure 7, in the upper layer the disturbance over the bump is relatively weaker. There is a small Taylor column in the slow region on the upstream equatorward side of the bump. The maximum flow acceleration occurs to the north-east and is a factor of about 3, compared with about 6 or 7 for the lower layer. At a radial distance of about $4L$ (200 km) to the north-east, in both layers, there is a cyclonic meander that is a general characteristic of the prograde solutions. Its strength is somewhat less in the upper layer. To the south-east, there is accelerated flow at a radial distance of $6L$ (300 km), with the flow velocity about doubled and directed towards the north-east. The maximum north–south meander amplitude is about $8L$ (400 km) in the lower and $7L$ (350 km) in the upper layer. For a larger value of h_0/ϵ, additional closed eddies occur: for $h_0/\epsilon = 8\cdot0$ (1013 m), there is a cyclonic eddy to the north-east in the lower layer, while for $h_0/\epsilon = 10\cdot0$ (1267 m) it occurs in both layers.

The interface contours, figure 1 (c), are geometrically similar to the streamlines, except right over the bump. Associated with a cyclonic meander is a locally raised interface, while associated with an anti-cyclonic meander is a locally depressed interface. For cases when a cyclonic eddy occurs, there can be an associated closed interface contour, indicating a domed interface within the cyclonic eddy. For a sufficiently tall bump, an anti-cyclonic eddy can form to the south-east, with an associated closed interface contour indicating a depressed interface within the anti-cyclonic eddy.

These trends continue as h_0/ϵ is further increased. For sufficiently large h_0/ϵ, the domed interface can surface, at which point the analysis breaks down, unless the governing equations are constrained to $-0\cdot8 < \eta < +0\cdot2$. This is because there is a limit to how much a fluid column in either layer can be stretched. Once the interface surfaces, the surface streamlines correspond to a cyclonic current ring with a slower cold (lower layer) core.

The asymptotic wavelength λ associated with the wavy part of (5.2) is

$$\lambda = 2\pi L/k_1,$$

which for the example works out at about 575 km.

A last piece of information is the wave drag D on the bump due to the wake. Again this is expressed by a drag coefficient C_D calculated from integration of the pressure distribution on the bump surface. The calculation yields

$$C_D \equiv \frac{D}{\rho_0 U_0 f_0 L^3} = \left| 4\epsilon\delta \left(\frac{h_0}{\epsilon}\right)^2 J_1[k_1] [N_2 + k_1^2] \frac{C_0}{d} \right|. \tag{5.9}$$

For the example, this coefficient is $0\cdot0406$, giving an actual drag of $0\cdot643 \times 10^{16}$ dynes. If this were a wind-driven current, with a surface stress of say 2 dynes cm^{-2} driving it, then the wave drag would be sufficient to balance the surface force on a square of side about 570 km.

6. Experiments related to the single-layer problem

Some pertinent experimental work was done by Fultz & Long (1951), Long (1952), Frenzen (1955) and Fultz & Frenzen (1955). Their basic apparatus was a hemispherical annulus, within which an obstacle could be moved along a

latitude circle. Most of the work was concerned with obstacles that completely filled the gap height. But Long (1952) reported results for a circular obstacle (10° angular radius), which was a half-gap width high. In terms of the parameters of the present work, with $U_1 = d = 1$, the sample photograph Long presented (his figure 11) corresponds to $\epsilon = 0.29$, $b = 0.612$, $h_0/\epsilon = 1.75$, and prograde flow. His photograph closely resembles the present figure 4 (a) ($b = 1$ and $h_0/\epsilon = 2.0$), with the slowest flow shifted towards the front of the obstacle, anti-cyclonic circulation around the bump, and the largest deflexion equatorward of the streamlines in the wake occurring at approximately 2 to $2\frac{1}{2}$ obstacle radii (from figure 4 (a), the corresponding length is just over 2 for $b = 1$). For retrograde flow, he reported that there was anti-cyclonic circulation about the obstacle, but that "...this has little effect on the motion in the rest of the hemispherical shell". It is not clear from this statement whether he means that there was only a small disturbance away from the obstacle (as the present theory would predict (figure 2)), or that the flow field was similar to that for the full cylindrical obstacle, which he described as having a blocked zone moving at the speed of the obstacle, with stagnant fluid outside the latitude zone of the obstacle.

To clarify this point, and to examine the experimental features, a set of experiments was run. The apparatus used was a large (1 m radius) rotating table, around which various small obstacles could be towed along constant radius curves. Since the fluid surface was free (parabolic), the effective β was a function of R. Hence any comparisons with the present theory are only approximate (i.e. only valid in a band of limited radial extent). Flow visualization was achieved by attaching a number of conducting wires to the obstacle support arm, and using the Baker (1966) thymol dye technique.

Figure 8 (plates 1 and 2) shows photographs of the prograde flow field for $\epsilon = 0.10$, $h/\epsilon = 3.0$, $b = 0.504$ and $E^{\frac{1}{2}} = 2.9 \times 10^{-2}$. The obstacle is moving by the camera. Figure 8 (a) (plate 1) shows the flow over the disk, and indicates excellent qualitative agreement with the theory (no theoretical streamlines were computed for $b = 0.5$). The wriggling of the dye lines was caused by the small Kármán vortex streets behind the dye wires. This has the effect of oscillating the effective radial dye release location and, owing to the divergence of streamlines in the slow flow regions, making the flow within the slow regions appear irregular.

Figure 8 (b) (plate 2) shows more of the wake, showing the meander amplitude to be of the order of L, and that the maximum streamline deflexion occurs at approximately 2·5–3 times L. From figure 4 (a), for $b = 1.0$ the corresponding number is 2·1 times L; and, for smaller b, we should get a value somewhat greater than this, agreeing with the observation. The crowding of the lower 6 streamlines in the wake is caused by the dye wires for those 6 lines being located in a relatively stagnant region: from the spacings, the velocities to the south-west of the disk are about $\frac{1}{2}$ to $\frac{1}{3}$ of their value in the first meander in the wake. This, too, is in good agreement with figure 4 (a).

In figure 9 (plate 3) a case is shown for which $\epsilon = 0.07$, $b = 1.1$, $h/\epsilon = 5.3$ and $E^{\frac{1}{2}} = 3.2 \times 10^{-2}$. There is a cyclonic eddy to the north-east at a radius of about $2L$, in good agreement with figure 4 (c). The flow in the slow region over

the disk is rather irregular, being influenced by viscosity and the support shaft.

For retrograde flows, two distinct regimes were observed. For relatively short obstacles, the streamlines were similar to those shown in figure 2, with some east–west asymmetry due to viscous drag. For taller obstacles, the flow was no longer stationary. Instead, the latitudinal band that the obstacle traversed blocked, with the fluid in the band moving with the obstacle, and the fluid outside the band being nearly stagnant. Superimposed on the shear layers at the edges of the band were large vortices, moving at some intermediate speed. The blocked region can be explained by Rossby wave theory: the linearized time-dependent equations of motion on a β plane have a wavy solution, which has westward group velocity and zero x wavenumber (see Lighthill 1967). The resultant shear layers are unstable, and could roll up into the observed vortices. Why this blocking does not occur all the time is under investigation. It may be related to the minimum height $(h_0)_c$ for formation of a Taylor column: if $h_0 < (h_0)_c$, the fluid can flow freely over the bump, and perhaps then the necessary forcing for the blocked flow does not occur.

The prograde flow experiments show excellent qualitative agreement with the theory of § 5. An important conclusion is that the use of the $r^{\frac{1}{2}}\phi \to 0$ upstream condition in the theory seems justified: the meandering wakes were found on the downstream side in all cases. It would be of interest to do more quantitative experiments, with the following aims: to make a detailed comparison with theory (critical height for Taylor-column formation, and meander amplitudes); to determine when the meandering wakes are stable; to determine when the embedded eddies in the wake are stable (e.g. are there situations in which these eddies get swept downstream?); to determine the effect of time dependence (e.g. slowly varying the translation speed of the bump). Further work on time-dependent vortex shedding would also be of interest. Some of these things are under investigation by the author at the Woods Hole Oceanographic Institution.

7. Conclusions and geophysical implications

The effect of variable Coriolis parameter on inertial-Taylor-column formation has been determined for a two-layer stratified fluid on a β plane. A special case of the solutions obtained corresponds to Taylor-column formation in a single-layer fluid: the β-plane extension of Ingersoll's (1969) study. The solutions for this special case have the following features.

(i) The pronounced cross-stream asymmetry of the flow streamlines found by Ingersoll (1969) also occurs on the β plane (figures 2, 4). In Ingersoll's case, the circulation around the bump was always anti-cyclonic. In the present case, it was always anti-cyclonic for a retrograde (westward) basic flow (4.7), but for a prograde (eastward) basic flow it could be cyclonic (5.5).

(ii) For the retrograde (westward) basic flows, the effect of β is to limit the radial extent of the disturbance to the basic zonal flow. This is in contrast to Ingersoll's (1969) f-plane solution. The streamline pattern is still upstream–downstream symmetric (figure 2), however.

(iii) For the prograde (eastward) basic flows, an extensive meandering wake is found downstream of the bump (figure 4). This wake decays downstream only like $r^{-\frac{1}{2}}$. Associated with the meander pattern there can be eddies: cyclonic eddies to the downstream poleward side and anti-cyclonic to the downstream equatorward side, and also accelerated jet-like regions.

(iv) The upstream–downstream asymmetry of the prograde solutions leads to a drag force on the bump: a wave drag. This can be calculated explicitly ((5.6), figure 5).

(v) Some simple experiments were done, which confirm the general character of the prograde flow solution (figures 8 (plates 1, 2) and 9 (plate 3)), and in particular the validity of the no upstream wave condition used in the solutions. For retrograde flow, streamlines similar to the theory are sometimes seen; but at other times the latitudinal band at the bump blocks, and time-dependent vortex shedding is observed.

These phenomena also occur in the full two-layer solutions: so long as the velocities in each layer are in the same direction, the primary effect of the stratification is to attenuate the Taylor-column strength in the upper layer (figure 7). This bottom-trapping, which for $S \to \infty$ becomes 100 %, is the two-layer analogy of Hogg's (1973) Taylor 'cones' for a linearly stratified f-plane system.

The amplitude of the meandering wake in the prograde flow example shown in figure 7 is nearly the same in the two layers. In §5 this was shown to be a general conclusion, so long as b/S was $\lesssim 1$.

When the basic flow was a counter-flow, the situation was found to be more complicated (§3). Even for $b = 0$, the solutions had a wavy character: a stationary baroclinic wave forced by the bump. In §3 it was shown that, for non-zero b, two wavy modes can exist; and the appropriate boundary conditions for each mode were determined (see discussion of (3.4) and (3.5)). It is also possible for two wavy modes to occur when both layers are prograde (tables 2, 3).

Hogg (1973) summarized the little, mostly indirect, evidence for Taylor columns. The evidence is of two types. The first type is observations of anti-cyclonic vorticity above seamounts, either direct, by neutrally buoyant float tracks, or indirect deduction from detailed hydrographic stations. The second type is a large body of indirect geological evidence: asymmetric sediment distributions, current scouring, and moats observed on and near seamounts. The reader is referred to Hogg's paper for the specific references. The best plan of attack for future attempts at observation is probably the tracking of an array of surface drifters and/or neutrally buoyant floats, preferably in a region with a relatively smooth approaching flow (i.e. not near the Gulf Stream) and with a single dominant bottom topographic feature, well isolated from other large bumps.

The most familiar example of a large-scale meandering current is the Gulf Stream. The forcing due to the New England Seamount Chain may play a role in these meanders, although the inherent instabilities and time dependence of the Gulf Stream render it impossible to make a strong statement. Quite often (Fuglister 1963; Fuglister & Voorhis 1965; Hansen 1970; Fuglister 1972; Robinson, Luyten & Fuglister 1974), the particular segment of the Gulf Stream path that crosses the Chain has anticyclonic curvature. There is also an observa-

tion of the formation of a cyclonic eddy ('Edgar') downstream from one of these anti-cyclonic crossings of the ridge (Fuglister & Worthington 1951).

Another possible example of meandering downstream from a topographic feature was described by Gordon & Bye (1972), who, in discussing a chart of dynamic topography of the Southern Ocean, pointed out that there are two regions where the contours meander. One is downstream from the Campbell Plateau and the other downstream from the USARP fracture zone. They find that the observed wavelength, combined with the stationary Rossby wave dispersion relation, predicts a flow velocity consistent with the observed flow speeds. The present theory shows the role the bottom topography plays in forcing these meanders. Indeed, the dynamic topography they show at the tip of the Campbell Plateau and over the USARP fracture zone shows anti-cyclonic curvature. Owing to the large scales involved, and the logistic difficulties, further observations here might be best made by satellite-tracked surface drifters.

In §5, the wave drag for the two-layer example illustrated in figure 7 was computed to be nearly 10^{16} dynes. The wave drag associated with prograde flows interacting with large-scale topography is thus big enough to contribute to the overall momentum balance of the current system. Munk & Palmén (1951) noted that the wind stress driving the Antarctic Circumpolar Current is of the order of 10^{17} dynes. A model current, which balances wind stress against only lateral and/or bottom friction, requires rather unpleasantly high eddy-viscosity coefficients. Munk & Palmén (1951) found the necessary horizontal coefficient to be of the order of $10^{10}\,\mathrm{cm^2\,s^{-1}}$. They suggested that a combination of bottom friction and 'mountain effect' (i.e. pressure drag of the kind described in §5) might be a more reasonable model. More recent theoretical work has somewhat reduced the viscosities needed for a friction-controlled model: Gill (1968) found that either $10^8\,\mathrm{cm^2\,s^{-1}}$ for a lateral coefficient or $10^3\,\mathrm{cm^2}$ for a vertical coefficient yielded reasonable current magnitudes. The 10^{16} dynes mentioned above suggests that Munk & Palmén were correct, and that any future theoretical modelling projects for the Antarctic Circumpolar Current should include some form of mesoscale topography, rather than artificially large eddy coefficients.
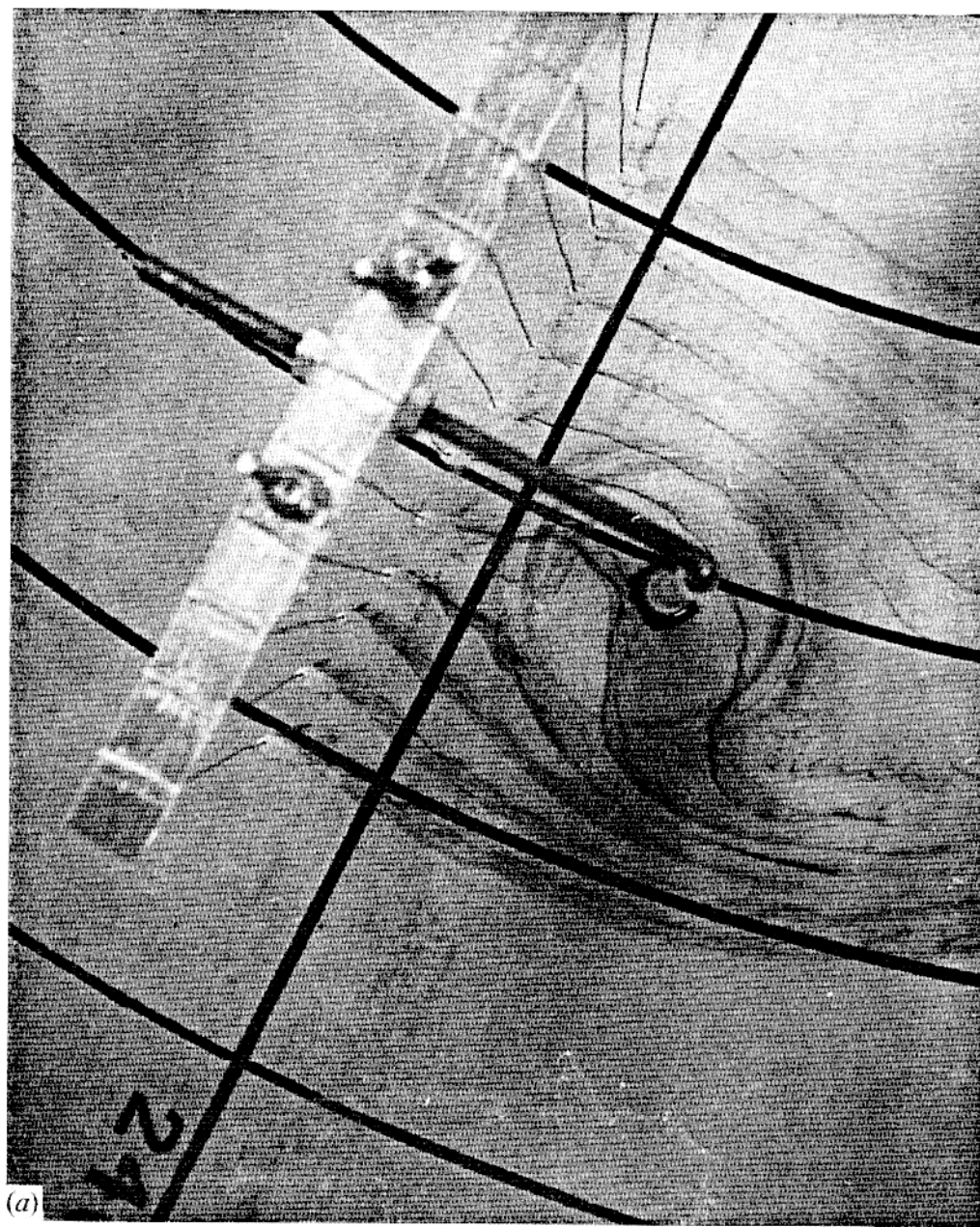
FIGURE 8(a). For legend see plate 2.

FIGURE 8. Experimental streamlines for $\epsilon = 0.10$, $b = 0.504$, $E^{\frac{1}{2}} = 0.029$ and $h_0/\epsilon = 3.0$. (b) was taken at a slightly later time than (a), as the bump moved by beneath the camera, and thus shows more of the wake.
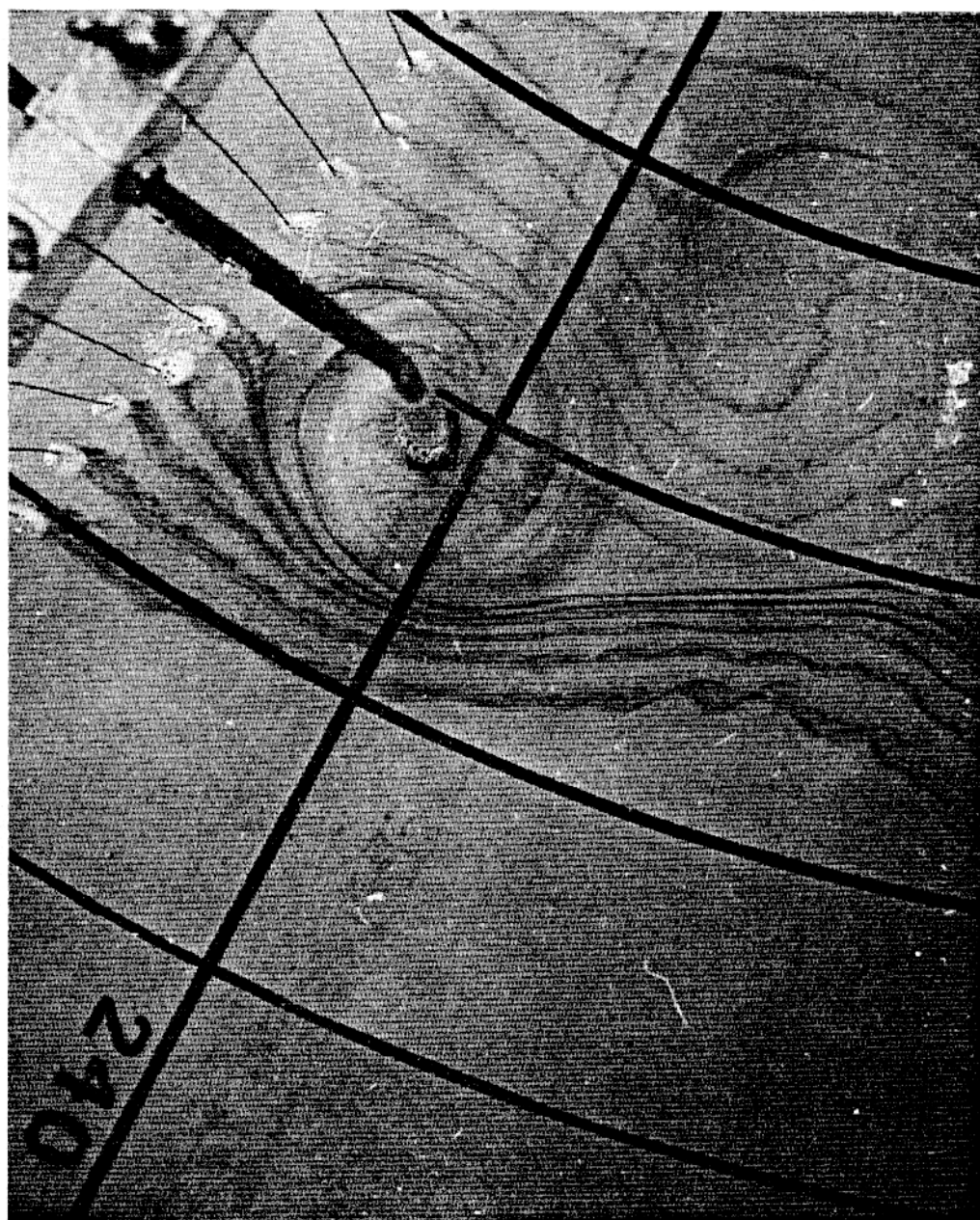
McCARTNEY

FIGURE 9. Experimental streamlines for $\epsilon = 0.07$, $b = 1.10$, $E^{\frac{1}{2}} = 0.032$ and $h_0/\epsilon = 5.3$.

REFERENCES

BAKER, D. J. 1966 A technique for the precise measurement of small fluid velocities. *J. Fluid Mech.* **26**, 573–575.

FRENZEN, P. 1955 Westerly flow past an obstacle in a rotating hemispherical shell. *Bull. Am. Met. Soc.* **36**, 204–210.

FUGLISTER, F. C. 1963 Gulf stream '60. *Prog. in Oceanography*, **1**, 265–383.

FUGLISTER, F. C. 1972 Cyclonic rings formed by the Gulf Stream 1965–66. *Studies in Physical Oceanography: a Tribute to Gieorg Wust on his 80th Birthday*, pp. 137–168. Gordon & Breach.

FUGLISTER, F. C. & VOORHIS, A. D. 1965 A new method of tracking the Gulf Stream. *Limnol. Oceanog. Suppl.*, **10**, R 115–R 124.

FUGLISTER, F. C. & WORTHINGTON, L. V. 1951 Some results of a multiple ship survey of the Gulf Stream. *Tellus*, **3**, 1–14.

FULTZ, D. & FRENZEN, P. 1955 A note on certain interesting ageostrophic motions in a rotating hemispherical shell. *J. Meteor.* **12**, 332–338.

FULTZ, D. & LONG, R. R. 1951 Two-dimensional flow around a circular barrier in a rotating spherical shell. *Tellus*, **3**, 61–68.

GILL, A. E. 1968 A linear model of the Antarctic circumpolar current. *J. Fluid Mech.* **32**, 465–488.

GORDON, A. L. & BYE, J. A. T. 1972 Surface dynamic topography of Antarctic Waters. *J. Geophys. Res.* **77**, 5993–5999.

GRACE, S. F. 1927 On the motion of a sphere in a rotating liquid. *Proc. Roy. Soc.* A **113**, 46–77.

HANSEN, D. V. 1970 Gulf Stream meanders between Cape Hatteras and the Grand Banks. *Deep Sea Res.* **17**, 495–511.

HIDE, R. 1961 Origin of Jupiter's Great Red Spot. *Nature*, **190**, 895–896.

HOGG, N. G. 1973 On the stratified Taylor column. *J. Fluid Mech.* **58**, 517–537.

HUPPERT, H. E. 1975 Some remarks on the initiation of inertial Taylor columns. *J. Fluid Mech.* **67**, 397–412.

INGERSOLL, A. P. 1969 Inertial Taylor columns and Jupiter's Great Red Spot. *J. Atmos. Sci.* **26**, 744–752.

JACOBS, S. J. 1964 The Taylor column problem. *J. Fluid Mech.* **29**, 581–591.

LIGHTHILL, M. J. 1967 On waves generated in dispersive systems by travelling forcing effects, with applications to the dynamics of rotating fluids. *J. Fluid Mech.* **27**, 725–752.

LONG, R. R. 1952 The flow of a liquid past a barrier in a rotating spherical shell. *J. Meteor.* **9**, 187–199.

McCARTNEY, M. S. 1972 Taylor columns and Rossby wakes generated by isolated topographic features on a beta-plane. *Notes on the 1972 Summer Study Program in Geophysical Fluid Dynamics at the Woods Hole Oceanographic Institution, WHOI Ref.* 72–79, 60–81.

MILES, J. W. & HUPPERT, H. E. 1968 Lee waves in a stratified flow. Part 2. Semi-circular obstacle. *J. Fluid Mech.* **33**, 803–814.

MUNK, W. H. & PALMÉN, E. 1951 Note on the dynamics of the Antarctic Circumpolar Current. *Tellus*, **3**, 53–56.

PEDLOSKY, J. 1964 The stability of currents in the atmosphere and the ocean. Part 1. *J. Atmos. Sci.* **21**, 201–219.

ROBINSON, A. R., LUYTEN, J. R. & FUGLISTER, F. C. 1974 Transient Gulf Stream meandering. Part 1. An observational experiment. *J. Phys. Oceanog.* **4**, 237–255.

STEWARTSON, K. 1953 On the slow motion of an ellipsoid in a rotating fluid. *Quart. J. Mech. Appl. Math.* **6**, 141–162.

STEWARTSON, K. 1967 On slow transverse motion of a sphere through a rotating fluid. *J. Fluid Mech.* **30**, 357–369.

VAZIRI, A. & BOYER, D. L. 1971 Rotating flow over shallow topographies. *J. Fluid Mech.* **50**, 79–95.